narra j

Original Article

Ethanol extract from *Ziziphus nummularia* stem inhibits MCF-7 breast cancer cell proliferation through TP53 regulating kinase (TP53RK)-mediated p53 activation: In silico and genes expression investigations

Berna Elya[1], Rosmalena Rosmalena[2], Ajeng M. Fajrin[2], Aryo Tedjo[2,3,4*], Nur A. Ramadanti[3], Norma N. Azizah[4] and Najihah BM. Hashim[5]

[1]Department of Pharmacognosy, Phytochemistry, and Natural Products, Faculty of Pharmacy, Universitas Indonesia, Jakarta, Indonesia; [2]Department of Medical Chemistry, Faculty of Medicine, Universitas Indonesia, Jakarta, Indonesia; [3]Master Program in Biomedical Sciences, Faculty of Medicine, Universitas Indonesia, Jakarta, Indonesia; [4]Drug Development Research Cluster, Indonesian Medical Education and Research Institute, Faculty of Medicine, Universitas Indonesia, Jakarta, Indonesia; [5]Department of Pharmaceutical Chemistry, Faculty of Pharmacy, Universiti Malaya, Kuala Lumpur, Malaysia

*Corresponding author: aryo.tedjo@ui.ac.id

Abstract

The p53 signaling pathway plays a critical role in regulating the cell cycle, apoptosis, and senescence, making it a key target in cancer research. The aim of this study was to investigate the effects of an ethanol extract from the stem of *Ziziphus nummularia* on the proliferation and expression of genes involved in the p53 pathway in MCF-7 breast cancer cells. To achieve this, real-time quantitative PCR (RT-qPCR) was used to evaluate the mRNA expression of downstream genes linked to cell cycle and senescence, including *CycE* or *CCNE1, RBL1, and E2F1*. Molecular docking simulations using Molegro Virtual Docker (MVD) were also performed to assess the potential inhibitory activity of metabolite compounds from *Z. nummularia* stem against p53-regulating kinase (TP53RK). The results showed that the IC_{50} value of *Z. nummularia* stem ethanol extract against MCF-7 cells was 38.27±0.72 µg/mL. The results also revealed a reduction in the expression of downstream genes linked to cell senescence and the cell cycle: *CycE* or *CCNE1* (p=0.011), *RBL1* (p=0.008), and *E2F1* (p=0.005), which was observed through RT-qPCR analysis of mRNA expression. This fact indicated that the inhibitory effects on proliferation by the ethanol extract of *Z. nummularia* stem might occur via pathways associated with cell senescence and cell cycle arrest. Molecular docking results of metabolite compounds from *Z. nummularia* stem suggested that squalene (Rerank score -112.70 kJ/mol), and nummularine B (Rerank score -110.68 kJ/mol) had potential as TP53RK inhibitors. These Rerank scores were smaller compared to the Rerank score of adenyl-imidodiphosphate (AMP-PNP), which was the native ligand of TP53RK, as confirmed by molecular dynamics analysis. These in silico results were confirmed by the decrease in *p21* (*CDKN1A*) mRNA expression. In conclusion, the anti-proliferative effects of the ethanol extract from *Z. nummularia* stem on breast cancer cells occurred by affecting cell cycle-related genes and inhibiting apoptosis protection mediated by overexpression of *p21* (*CDKN1A*) through p53 activity.

Keywords: TP53RK, *Ziziphus nummularia*, MCF-7, apoptosis, cell cycle arrest

Introduction

Breast cancer continues to be a significant global health issue with increasing mortality rates. According to the Global Burden of Cancer, the number of deaths due to breast cancer continues

Copyright: © 2025 by the authors. This is an open access article distributed under the terms and conditions of the CC BY-NC 4.0.

https://narraj.org/

Received: August 27, 2024 - Accepted: January 30, 2025 - Published online: February 10, 2025

to rise each year, with approximately 2.3 million new cases diagnosed and 685,000 deaths worldwide [1]. Based on hormone receptor expression, the most common classifications include four subtypes: luminal A, luminal B, HER2-positive, and triple-negative. Luminal A breast cancer was generally associated with low metastatic potential and a favorable prognosis. However, some patients with luminal A breast cancer have been found to develop metastasis in lymph nodes [2].

Current treatment options for luminal A breast cancer include surgery, chemotherapy, and endocrine therapy. Endocrine therapy has a favorable toxicity profile and is indicated as a first-line treatment for luminal A breast cancer [3], although long-term use of tamoxifen can lead to side effects such as endometrial cancer and thromboembolic disease [4]. Additionally, this type of breast cancer could develop resistance to endocrine therapy [5,6]. Therefore, it remains necessary to explore alternative anticancer therapies that target both endocrine receptors and other mechanisms, such as apoptosis.

Apoptosis, or regulated cell death, is a crucial mechanism in anticancer therapy. This mechanism aims to eliminate damaged or unwanted cells without causing damage to surrounding tissues [7]. In cancer, there is a progressive decrease in the ability of cells to trigger apoptosis, while in aging tissues, there is an accumulation of senescent cells [8]. Major anticancer drugs primarily target apoptotic signaling pathways to induce cancer cell death and prevent chemoresistance [9]. One signaling pathway that regulates apoptosis is the p53 signaling pathway. The *TP53* gene, which codes for the p53 protein, is known as a tumor suppressor gene. The transcription factor activated p53 is implicated in cell senescence, autophagy, DNA repair, apoptosis, and cell cycle regulation [10].

Apoptosis mediated by p53 activity is known to be capable of killing cancer cells, while p53-induced premature aging promotes tumor regression in vivo [11,12]. The TP53-regulating kinase (TP53RK), or PRPK, is essential for the activation of p53. However, the elevated TP53RK expression was linked to a poor prognosis in individuals with colorectal adenocarcinoma and multiple myeloma (MM) [13, 14]. The results of proteomic research showed that MCF-7 breast cancer cells greatly express TP53RK [15]. Knockdown of TP53RK was known to inhibit p53 phosphorylation and induced MM cell apoptosis [16]. Furthermore, the pharmacological inhibition of p53 phosphorylation through TP53RK could be achieved with immunomodulatory drugs (IMiDs) such as pomalidomide, which induces apoptosis by downregulating p53 phosphorylation (p-p53) by directly binding to TP53RK and inhibiting its kinase activity [16].

In wild-type p53 MM cells, thalidomide and its analogs are also known to reduce *p21* expression, facilitating the G1-to-S transition and increasing vulnerability to apoptosis [15]. It is known that the process of repairing DNA damage through apoptosis or cell senescence can be triggered by G1/S and G2/M transitions [17]. Based on the above explanation, the development of anticancer agents through TP53RK inhibition, including those derived from plants, is interesting to explore.

Ziziphus nummularia, or its synonym *Ziziphus rotundifolia*, a plant from the Rhamnaceae family, has shown potential as an anticancer agent [18]. This plant is rich in bioactive compounds such as cyclopeptide alkaloids, flavonoids, saponins, glycosides, tannins, and phenolic compounds [19]. It has been established that *Z. nummularia* ethanol extract inhibits pancreatic ductal adenocarcinoma cell proliferation in a concentration-dependent way [20]. Additionally, the extract decreased angiogenesis, downregulated signaling pathways linked to carcinogenesis and metastasis, and prevented cancer cells from migrating and invading [20]. Furthermore, *Z. nummularia* leaf extract-based gold nanoparticles have demonstrated anticancer efficacy against cell cultures of breast and cervical cancer [21]. These results implied the possibility of using *Z. nummularia* as a source of novel anticancer agent.

The administration of *Z. nummularia* extract has the potential to affect downstream TP53-related gene expression related to apoptosis and cell senescence. Research on other *Ziziphus* genera has shown that water and alcohol-water extracts of *Z. jujuba* can inhibit the proliferation of cervical and breast cancer cells and induce apoptosis by decreasing the expression of anti-apoptotic *Bcl2* genes and increased the expression of pro-apoptotic *Bax* genes [22]. Thyroid cancer C643 cell cultures were able to undergo apoptosis when exposed to water extract of *Z. jujube* [23]. Moreover, *Z. Spina*-christi leaf extract was known to trigger apoptosis by reducing *Bcl2* mRNA expression and increasing *Bax* mRNA expression in MCF-7 cells [24]. Several of the

previous results showed that the Ziziphus extract-treated breast cancer cells changed the expression of downstream *TP53* genes in apoptotic pathways [25,26]. This study will analyze changes in the expression of downstream *p53* signaling genes related to cell senescence and cell cycle arrest such as *CDKN1A* (*p21*), *CycE* (*CCNE1*), *RBL1*, and *E2F1* in MCF-7 breast cancer cells treated with ethanol extract of *Z. nummularia* stem. Molecular docking analysis of proteins related to TP53RK activity will also be conducted to explain which compounds *in Z. nummularia* stem are involved in influencing the mRNA expression of these genes. The aim of this study was to investigate the effects of an ethanol extract from the stem of *Ziziphus nummularia* on the proliferation and expression of genes involved in the p53 pathway in MCF-7 breast cancer cells. Through this approach, the binding affinity, complex stability, and key amino acid residues involved in ligand-protein interactions can be identified, providing insights into how compounds in *Z. nummularia* may inhibit or modulate the function of the target protein (TP53RK).

Methods

Materials and apparatus

The experimental materials were the stem fine powder of *Z. nummularia*, 96% ethanol (absolute ethanol) as the extraction solvent, MCF-7 cells, 10% fetal bovine saline (FBS) solution, penicillin-streptomycin, Dulbecco's modified eagle medium (DMEM), tamoxifen (positive control), and 2,5-diphenyl-2H-tetrazolium bromide (MTT) solution (5 mg/mL). Additionally, the tools and techniques employed consisted of ultrasonication for extraction, a rotary evaporator for concentration, a 96-well plate for cell viability assays, and reverse transcription-quantitative polymerase chain reaction (RT-qPCR) for gene expression analysis. The downstream p53 signaling pathway genes targeted for expression measurement were *CDKN1A* (*p21*), *CycE* (*CCNE1*), *RBL1*, and *E2F1*, with specific primer sequences from Macrogen, South Korea.

Extraction of *Z. nummularia* stem powder

The stem fine powder of *Z. nummularia* was cut into small pieces, dried, and powdered. A total of 50 g of the powder was added with absolute ethanol (96%) at a ratio of 1:10. Extraction was carried out using the ultrasonic method with 50°C and 40 kHz. The extraction process lasted for one hour. The solvent solution mixed with the powder was filtered to obtain the filtrate solution. The filtrate was then concentrated using a rotary evaporator (BUCHI RE300, Flawil, Switzerland) at 250 rpm for two hours.

Cell viability assay (microtetrazolium, MTT assay)

MCF-7 cells at a density of 5×10^3 cells/100 µL were placed in a 96-well plate with a medium containing 10% FBS solution, 1% penicillin-streptomycin, and 45 mL DMEM. Subsequently, 100 µL of *Z. nummularia* stem extract was added to MCF-7 cells and cultured for 24 hours at 37°C with 5% CO_2 in a serial concentration (500, 250, 125, 62.50, 31.25, 15.63, 7.81, 3.91, and 0.00 µg/mL) [27]. Incubation was also performed on MCF-7 cells given serial concentrations of tamoxifen as a positive control at the same concentration variation. Following the time of incubation, each well received 100 µL of a 5 mg/mL MTT solution. The MTT assay reaction was then stopped by adding a 10% SDS stopper after 6 hours. The incubation process was resumed in the dark overnight at room temperature. The results of the MTT assay reaction were appeared as a purple color, and its absorbance was measured using an ELISA reader at a wavelength of 595 nm. The absorbance data from each concentration of the test compound were used to construct a logarithmic dose-% inhibition curve. The IC_{50} value was determined using linear regression analysis and interpolation from the curve, where the intersection point corresponding to 50% inhibition of cell viability was identified. All experiments were performed in triplicate, and the results were presented as a percentage of cell inhibition compared to the control. The IC50 value was expressed in mean ± standard deviation (SD).

Real-time polymerase chain reaction (RT-PCR) analysis of downstream p53 signaling pathway gene expression

In order to assess gene expression, total RNA was extracted from MCF-7 cells treated with the extract at an IC_{50} dosage. The determination of the IC_{50} dose was performed using the MTT assay

for the extracted sample. Reverse transcription into cDNA was performed using 200 ng of extracted RNA and quantified using RT-qPCR. The primer for genes downstream of cell cycle arrest-related p53 signaling pathway or sequences for *CDKN1A* (*p21*), *CycE* (*CCNE1*), *RBL1*, and *E2F1* are presented in **Table 1**. Meanwhile, for the tamoxifen dose, the concentration dose was adjusted according to that reported previously (IC_{50}=25.79 µg/mL) [36].

Total RNA extraction and reverse transcription

Total RNA from MCF-7 cells was isolated using the FastPure® Cell/Tissue Total RNA Isolation Kit V2 (Vazyme, Nanjing, China). Then, 200 ng of the isolated RNA was reverse-transcribed into cDNA in preparation for qRT-PCR using the HiScript III RT SuperMix (Vazyme, Nanjing, China). FMR3 Real-Time Quantitative Thermal Cycler (Vazyme, Nanjing, China) and 2xTaq pro-Universal SYBR qPCR Master Mix (Vazyme, Nanjing, China) were used for the quantitative PCR process. To normalize the expression of the target genes, the *ACTB* gene was used as a housekeeping (HK) gene. Every sample was examined three times. The thermocycling program comprised two minutes of annealing at 94°C and 30 cycles of 30 seconds each at 94°C, 56°C, and 72°C. Subsequently, melting curve data were gathered to confirm the specificity of the PCR and the absence of primer dimers.

Table 1. Primers for genes downstream of cell cycle arrest-related p53 signaling pathway

Assay set	Type	Sequence (5' to 3')
CDKN1A	Forward primer	GAGTGTAGGGTGTAGGGAGATT
	Reverse primer	AGGAGGGAATTGGAGAGACTAC
CCNE1	Forward primer	TCCCAAAGTGCTGGGATTAC
	Reverse primer	CTACAAGCCTGAGCCACTATAC
RBL1	Forward primer	CTCTTTGCCTATAGCTCACCTC
	Reverse primer	GCGGATCACCACCTCAATAA
E2F1	Forward primer	GGTGAGAGCACTTCTGTCTTAAA
	Reverse primer	CACCAAAGAGGCCTCGATAAA
ACTB (housekeeping, HK)	Forward primer	TGACGTGGACATCCGCAAAG
	Reverse primer	CTGGAAGGTGGACAGCGAGG

Gene expression analysis

The expression values of the genes were expressed relative to the housekeeping gene (HK) using the Livak and Schmittgen method [28]. Relative quantification (R) was calculated as $R=2^{(-\Delta\Delta Ct)}$, where = ΔCt_sample – ΔCt_control = (Ct_target – Ct_HK) sample – (Ct_target – Ct_HK)_control, as recommended in a previous report [29]. Ct represents the cycle threshold, demonstrating the number of cycles the fluorescence signal needs to cross or exceed the threshold level.

Molecular docking and molecular dynamics simulations of compounds in *Z. nummularia* stem extract

The PubChem database was searched to obtain the 3D structures or conformations of the compounds in the *Z. nummularia* stem extract [19,30], and the results were recorded in the structure data file (SDF) format. Datawarrior v6.1.0 (openmolecules, Allschwil, Switzerland) [31] was used to minimize the energy of the 3D structures, and the file was saved in SDF format. The TP53RK-TP53RK binding protein (TPRKB) with AMP-PNP (PDB ID: 6WQX) ligand was downloaded from the RSCB PDB database (www.pdb.org) and saved as a Protein Data Bank (PDB) file [32]. Molegro Virtual Docker (MVD), a free trial version (Molegro, Aarhus, Denmark), was used for in silico testing [33]. The system used for the analysis included an Intel(R) Core(TM) i7-8665U CPU @ 1.90 GHz - 2.11 GHz processor, 16.0 GB RAM, and Windows 11 Pro specs.

Using MVD, the crystal protein structure that was retrieved from the RSCB PDB database was imported. All water molecules were eliminated, and noncompliant amino acid residues were fixed for the purpose of molecular docking. Datawarrior was used to prepare the ligands by determining the lowest energy or the most stable conformation (Merck Molecular Force Field, MMFF94 value).

Potential binding cavities or locations for ligand binding to TP53RK-TPRKB (PDB ID: 6WQX) were predicted using MVD. Two TP53RK or PRPK protein chains and TPRKB chains

were combined to form the complex protein. The ligand on two TP53RK protein chains known as AMP-PNP (adenyl-imidodiphosphate) is present in the crystal protein structure. The binding site for ANP_301 (AMP-PNP), a ligand presents on chain D in the crystal protein structure, had been determined to be a cavity with a volume of 193.024 $Å^3$ and a surface area of 593.92 $Å^2$. The center coordinates of the sphere containing this binding site were X: 0.00; Y: -11.60; Z: 50.84. The sphere had a radius of 11. A MolDock grid score was determined using a grid resolution of 0.30.

Z. nummularia stem extract was used to analyze the interactions between proteins and ligands through molecular docking. All 3D structures of the compounds or ligands were analyzed using molecular vibration detection (MVD) [19,26]. The docking approach was validated by re-docking the 3D molecule ANP_301 (AMP-PNP) in 6WQX [D] at the protein binding site area. The Root Mean Square Deviation (RMSD) value of less than 2 Å was established as the validity criterion for this method [34]. The 3D structure of the ligand was then fitted to the crystal protein structure using molecular docking. Pomalidomide (positive control), a thalidomide derivative that is known to directly interact with the TP53RK protein and suppress the production of p21 mRNA, was also subjected to molecular docking [16]. The energy values associated with this docking process, such as the Hbond, MolDock Score, and Rerank Score, were measured. Rerank Score is a frequently used metric to assess the degree of binding between the ligand and the receptor protein [35].

The molecular dynamics simulation of the complex resulting from docking was conducted using YASARA structure software version 23.12.24.W.64 (Biosciences GmbH, Vienna, Austria) over a period of 10.00 ns. After initial structural preparation (structural cleanup and pH adjustment), simulations were performed with YASARA, using the AMBER14 force field integrated into the YASARA structure (macro: md_run.mcr). To elaborate, the Poisson-Boltzmann approach is the technique chosen to manage the electrostatic force to obtain an electrostatic potential with an implicit solvent and counter ions. A "simulated cubic cell" was installed and flooded with water, maintaining a density of 0.997 g/mL and an isobaric pressure at 298 K. To mimic a neutral physiological environment, sodium chloride was introduced at a concentration of 0.9%. The distance between the protein and the cell boundary was set to 10 Å.

Statistical analysis

The relative gene expression levels obtained from RT-PCR were calculated using the 2^(-ΔΔCt) method. Statistical analysis of the RT-PCR results (gene expression level) was conducted using t-test to compare the treatment of each group to the control. Data were presented as mean±SD from at least three independent biological replicates (n=3), and a p-value <0.05 was used to determine statistical significance. All statistical analyses were performed using Microsoft Excel (Microsoft, Redmond, Washington, USA).

Results

Results from cell viability assay

The results of the MTT assay for the ethanol extract of *Z. nummularia* stem on MCF-7 cells are presented in **Figure 1**. It was evident that the extract exhibited a dose-dependent inhibition of proliferation, with the percentage of MCF-7 cell proliferation inhibition increasing as the administered dose increased. *Z. nummularia* stem ethanol extract's IC_{50} against MCF-7 cells was determined to be 38.27±0.72 µg/mL.

Gene expression analysis

The relative mRNA expression was found to differ significantly for *CDKN1A* (*p21*) (p=0.03), *CycE* (*CCNE1)* (p=0.011), *RBL1* (p=0.008), *and E2F1* genes (p=0.005) (**Figure 2A**). The relative mRNA expression of all four genes showed a decrease with the administration of the ethanol extract from *Z. nummularia*. On the other hand, only *E2F1* (p=0.011) and *RBL1* (p=0.017) exhibited significant differences in relative mRNA expression, as compared with the control (**Figure 2B**). The mRNA expression of *E2F1* gene was upregulated in the tamoxifen group, while it was downregulated for *RBL1* gene. The summarized fold change (FC) values for the extract and tamoxifen for each gene are presented in **Table 2**.

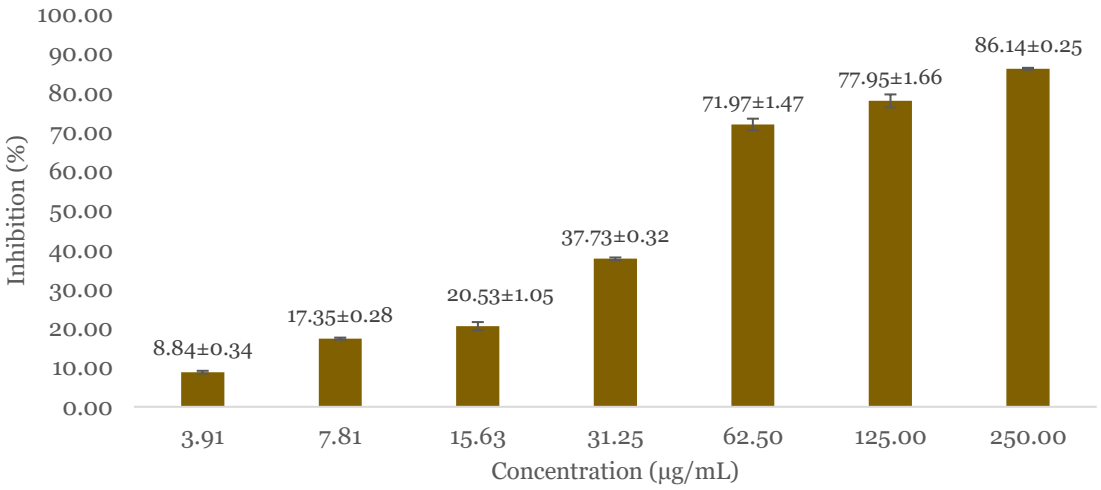

Figure 1. MTT assay to determine MCF-7 cell viability for various concentrations.

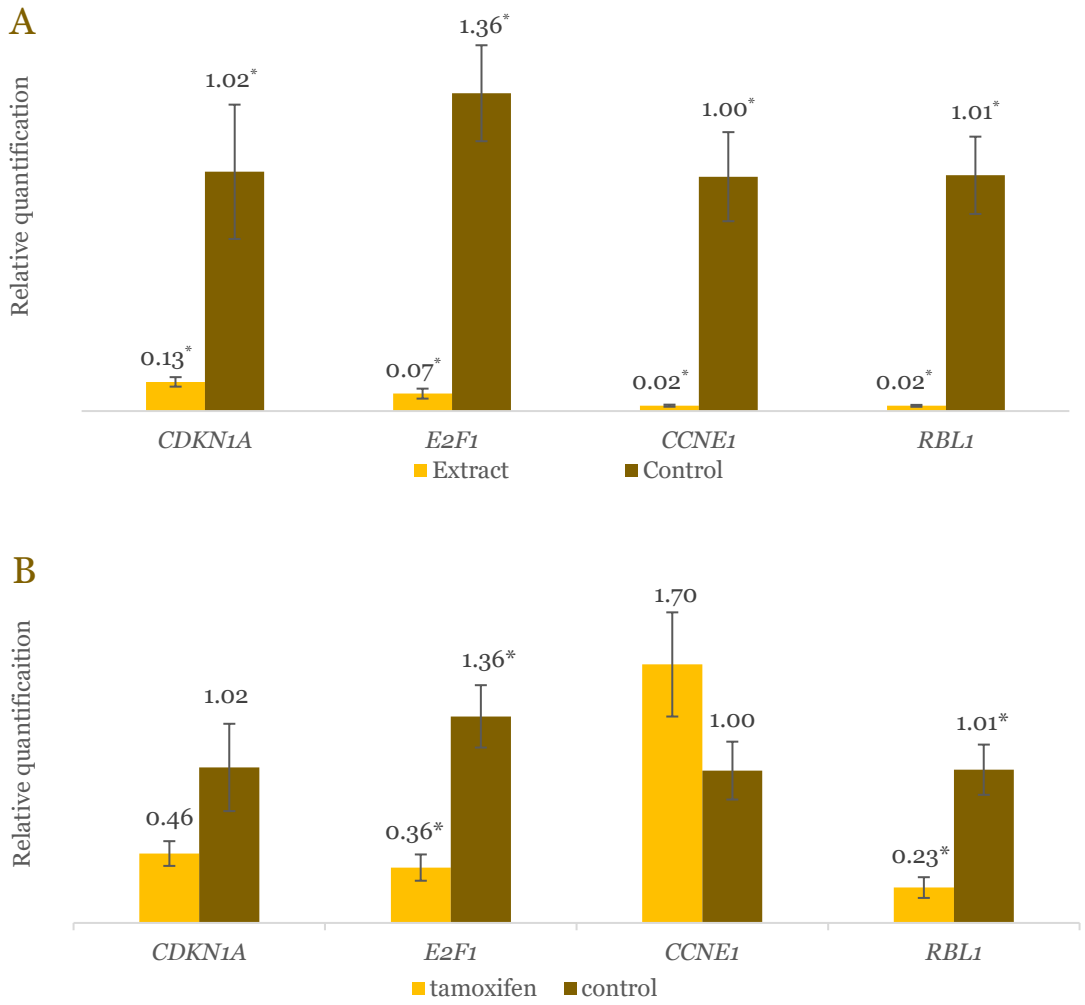

Figure 2. Relative mRNA expression or relative quantification (R) result. The figure illustrates the relative mRNA expression or relative quantification (R) presented in $2^{(-\Delta\Delta Ct)}$ between *Z. nummularia* stem ethanol extract vs control (A) and tamoxifen vs control (B). The asterisk (*) indicated a significant difference ($p<0.05$) between the treatment of MCF-7 cells with extract or tamoxifen administration (sample) and control (without sample administration).

Table 2. Fold change (FC) of relative quantification mRNA between sample (extract or tamoxifen) and control

Genes	FC (extract)	Regulation	*p*-value	FC (tamoxifen)	Regulation	*p*-value
CDKN1A	0.122	Down	0.030*	0.446	Down	0.070
E2F1	0.055	Down	0.005**	0.268	Down	0.011*
CCNE1	0.023	Down	0.011*	1.697	Up	0.060
RBL1	0.022	Down	0.008**	0.231	Down	0.017*

*Statistical significance at $p<0.05$
**Statistical significance at $p<0.01$

Molecular docking and molecular dynamics simulations

The validation findings of the interaction between TP53RK and its crystal structure ligand (AMP-PNP or ANP_301) during the redocking procedure are presented in **Figure 3** and **Table 3**. Several steric-electrostatic and hydrogen bonding interactions occurred at the same amino acid residues. The illustration of these interactions is presented in **Figure 4**. The redocking yielded RMSD values less than 2 Å in conformation 4 (**Table 3**), suggesting the grid box validity [37]. Subsequently, molecular docking was performed between the metabolite compounds in *Z. nummularia* (20 compounds) and pomalidomide with TP53RK (6WQX [D]). The results of molecular docking are presented in **Table 4** and **Figure 5**.

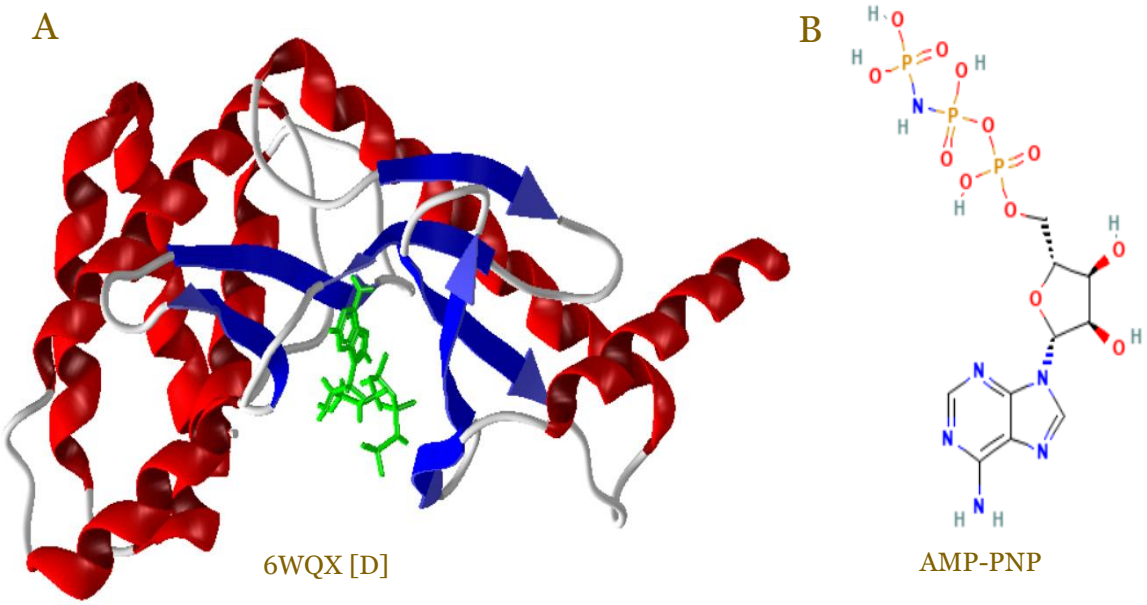

Figure 3. (A) 3D structure of TP53RK protein or 6WQX [D] and (B) AMP-PNP ligand in its 2D crystal structure.

Table 3. Released energy values (docking scores) from TP53RK (6WQX [D]) interaction with native ligand (AMP-PNP/ANP_301) and RMSD values from redocking

Conformation	MolDock score (kJ/mol)	Rerank score (kJ/mol)	RMSD (Å)	HBond (kJ/mol)
4	-140.329	-109.171	1.94886	-3.64051
2	-143.151	-70.4764	2.82858	-11.4409
0	-143.682	-100.228	4.36464	-13.2306
3	-134.339	-69.5526	6.29976	-10.5772
1	-146.565	-90.8776	7.97302	-9.4033

Based on the molecular docking results of 20 metabolite compounds in *Z. nummularia* with TP53RK, as listed in **Table 4**, three compounds exhibited lower (more negative) Rerank scores than ANP_301 (-110.35 kJ/mol), namely rutin (-113.69 kJ/mol), squalene (-112.70 kJ/mol), and nummularine B (-110.68 kJ/mol). In contrast, pomalidomide (-69.23 kJ/mol) showed a

significantly higher Rerank Score. Thus, these three compounds have the potential to act as TP53RK inhibitors.

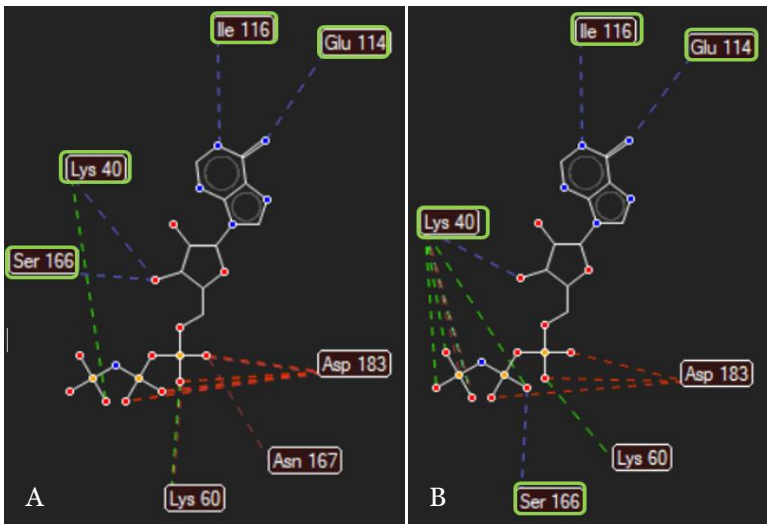

Figure 4. Interaction of TP53RK (6WQX [D]) with native ligand (AMP-PNP/ANP_301) in its crystal structure (A) and redocking (B). (-----) Hydrogen bonds; (-----) electrostatic interactions; (-----) steric interactions.

Table 4. Molecular docking results of metabolite compounds from *Ziziphus nummularia* with TP53RK in the optimal conformation

Ligand	MolDock score (kJ/mol)	Rerank score (kJ/mol)	Torsions	Hbond (kJ/mol)
Rutin	-131.14	-113.69	6	-17.01
Squalene	-149.98	-112.70	15	0.00
Nummularine_B	-150.62	-110.68	9	-3.62
ANP_301 [D]	-145.54	-110.35	8	-11.29
Scutianine_C	-150.05	-108.49	9	-1.94
Mauritine_D	-155.35	-106.05	10	-4.86
Chlorogenic acid	-109.83	-105.12	5	-15.23
Mauritine_F	-153.66	-103.19	7	-3.52
Nummularine_P	-153.48	-102.51	8	-0.52
Frangufoline	-133.37	-96.37	9	-1.68
mphibinine_H	-143.89	-95.90	9	-2.28
Phytol	-110.56	-86.89	13	-5.01
Quercetin	-87.34	-81.18	1	-11.20
Mauritine_A	-147.49	-79.24	8	-4.42
Lapachol	-85.02	-77.27	2	-4.34
Morin	-91.73	-76.41	1	-10.39
Pomalidomide	-77.97	-69.23	1	-4.06
Ethyl alpha-d- glucopyranoside	-60.90	-62.65	3	-15.40
Lupeol	-94.65	-58.23	1	-0.98
Mandelic acid	-63.06	-56.08	2	-8.60
Jubanine_B	-152.11	-53.02	11	-2.13
Pyrogallol	-53.00	-48.28	0	-12.47

The interaction results of rutin, squalene, nummularine B, and pomalidomide with TP53RK are presented in **Figure 5**. ANP_301 exhibited interactions involving hydrogen bonds with polar residues such as Ser166, Lys40, Ile166, and Glu114, which contribute to the stability of the compound-protein complex. Additionally, electrostatic interactions with Lys40 and steric interactions with Asp183 and Asn167 further enhanced the binding strength of this molecule within the active pocket of the protein. Rutin, which contains numerous hydroxyl (-OH) groups, formed multiple significant hydrogen bonds with residues such as Lys40, Ser166, Asn167, Ala45, Ile116, and Glu114. These interactions demonstrated that rutin heavily relies on polar bonds for stabilization.

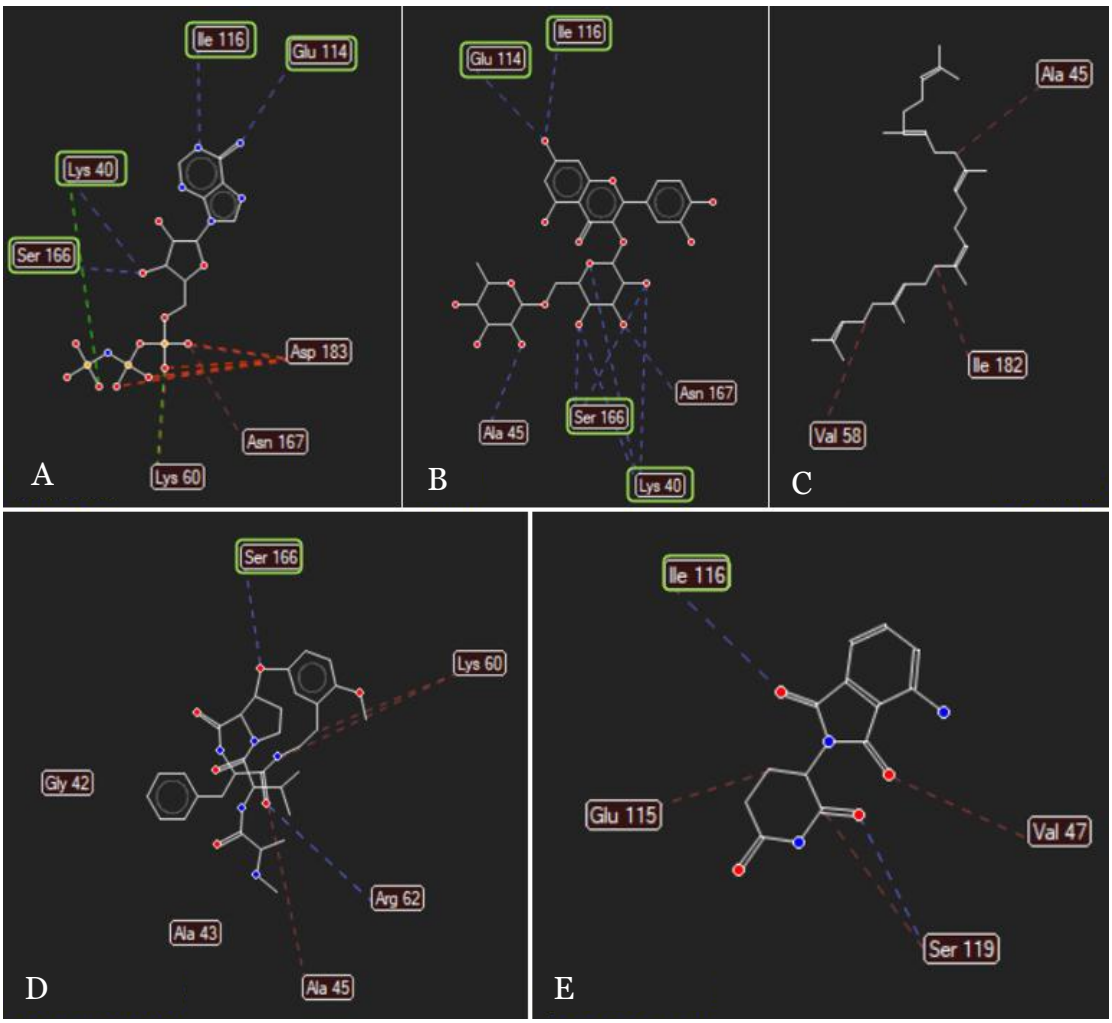

Figure 5. Interaction of TP53RK (6WQX [D])s with native ligand (A) on its crystal structure, rutin (B), squalene (C), and nummularine (D), as well as pomalidomide (E). (-----) Hydrogen bonds; (-----) electrostatic interactions; (-----) steric interactions.

Squalene, as a lipophilic molecule, primarily interacts through hydrophobic (steric) interactions with residues such as Val58, Ala45, and Ile182. The absence of hydrogen bonds suggests that the binding of squalene is predominantly dependent on non-polar interactions within the active pocket of the protein. Nummularine B exhibited a combination of hydrogen and hydrophobic (steric) interactions. This compound formed hydrogen bonds with polar residues such as Ser166 and Arg62, while simultaneously interacting with non-polar residues such as Gly42, Ala43, and Ala45, which provided additional stability to the compound-protein complex. Pomalidomide formed hydrogen bonds with polar residues such as Ile116 and Ser119, which enhanced its binding selectivity. Moreover, hydrophobic (steric) interactions with residues Val47 and Glu115 also contributed to the binding stability. The combination of hydrogen bonds and hydrophobic interactions explained the effective binding of pomalidomide, despite its higher Rerank Score compared to other compounds.

At 10 ns molecular dynamic simulation, the four protein-ligand complexes analyzed demonstrated stability after the initial few nanoseconds (2–3 Å) (**Figure 6**). When comparing the native ligand complex with the test compounds, the RMSD curve of the test compounds was lower than that of the native ligand. Root mean square fluctuation (RMSF) measures the extent to which each residue fluctuates during molecular dynamics simulation. When comparing the native ligand complex with the test compounds, the RMSF curve of the test compounds was lower than that of the native ligand, indicating relatively stable residues. Regarding the amino acid residues interacting with the ligand, all ligand complexes exhibited stable interactions with

several essential amino acids, such as Ile 116, Ile 182, Lys 40, Lys 60, Val 47, Val 58, and Arg 62 (**Figure 6**).

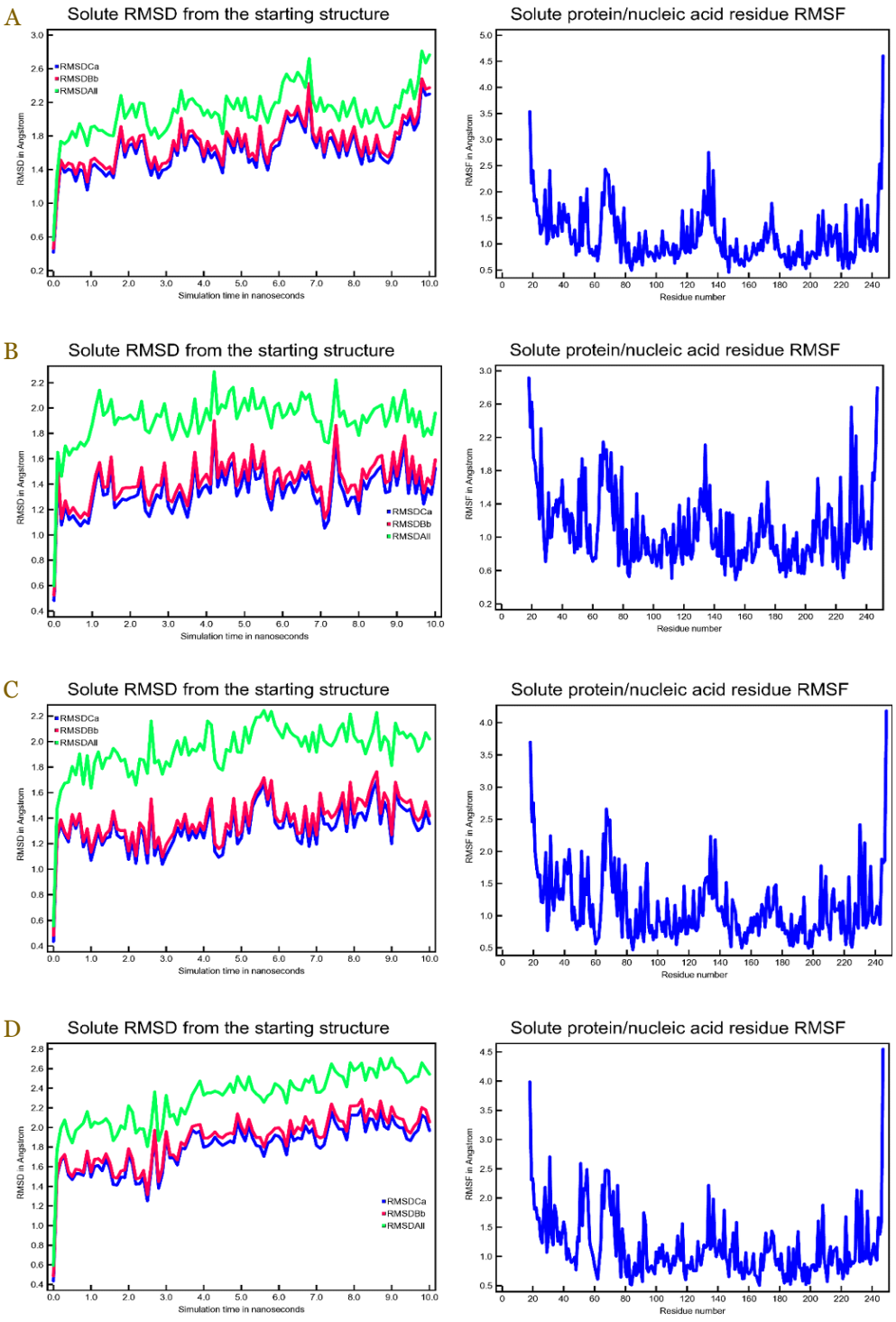

Figure 6. RMSD and RMSF curves of the complex compound in the 10-ns simulation: TP53RK-AMP-PNP Ligand (A), TP53RK-squalene (B), TP53RK-pomalidomide (C), and TP53RK-nummuraline B (D).

Discussion

In this present study, the anticancer potential of *Z. nummularia* stems was investigated through in silico analysis, demonstrating its effect on activation of the p53 signaling pathway via inhibition of TP53RK via p53-related protein kinase (PRPK). Based on the Rerank score results, three compounds in *Z. nummularia* stem, namely rutin, squalene, and nummularine B, have the

potential to act as TP53RK inhibitors. MVD recommends the use of Rerank score to evaluate the results of molecular docking. A lower (more negative) Rerank score compared to the native ligand indicates that the binding between the tested compounds (rutin, squalene, and nummularine B) and the target protein (TP53RK) is stronger or more stable. In the context of molecular docking, a more negative score typically correlates with lower binding energy, implying that the compound-protein complex is more energetically stable than the native ligand. From a biological perspective, this is significant because compounds with higher binding affinity (more negative scores) are more likely to act as effective inhibitors. In this case, rutin, squalene, and nummularine B exhibit potential as TP53RK inhibitors, which could influence its biological activity. The molecular dynamics analysis results indicated that the RMSD and RMSF values of the test compounds (squalene, pomalidomide, and nummuraline B) are lower than those of the native ligand (AMP-PNP). A lower RMSD value, without significant residue fluctuations (lower RMSF), suggests that the system has achieved better equilibrium or structural stability. This finding aligns well with the molecular docking results, where squalene and nummuraline B have more negative Rerank scores, indicating more stable interactions with TP53RK compared to AMP-PNP.

The inhibition of the p53 signaling pathway is anticipated to impact downstream genes, particularly those involved in cell aging and cell cycle arrest. In this study, the genes associated with these processes, namely *CDKN1A* (*p21*), *CycE* (*CCNE1*), *RBL1*, and *E2F1*, significantly down-regulated in MCF-7 cells following the administration of ethanol extract from *Z. nummularia* stem. TP53RK plays a critical role in regulating p53 phosphorylation and promotes the activation of downstream genes like *CDKN1A* and *CCNE1*. *CDKN1A* encodes p21, a cyclin-dependent kinase inhibitor that halts the cell cycle at the G1/S transition by inhibiting CDK2 activity, while reduced expression of *CCNE1* (encoding cyclin E) further supports cell cycle arrest. Through these mechanisms, TP53RK inhibition indirectly modulates p53 activity, leading to controlled cell cycle progression and potential anticancer effects. Conversely, with tamoxifen treatment, only *E2F1* and *RBL1* demonstrated reduced mRNA expression. *E2F1, RBL1*, and *CCNE1* are genes whose expressions can serve as markers in cancer cells or patient prognosis. Most cancer cells have high expression levels of the transcription factor *E2F1*, which controls the development of the cell cycle and activates cell cycle-related transcription kinases [38].

Similar to *E2F1, RBL1* is a transcription factor involved in a cyclin domain resembling *CCND1* and *CCNE1*, and it is positively expressed in various types of cancer [39]. Patients with high *CCNE1* expression have a worse prognosis compared to those with low expression in ovarian, breast, gastric, lung, and liver cancers [40]. Thus, the significant down-regulation of *CCNE1*, *E2F1*, and *RBL1* expression with ethanol extract treatment from *Z. nummularia* stem is relevant to the cascade of cell aging and cell cycle arrest pathways mediated by p53, ultimately leading to cell cycle arrest. In contrast, tamoxifen appears to have a limited role in influencing aging and cell cycle arrest pathways mediated by the p53 signaling in MCF-7 cells.

CDKN1A (*p21*) serves as a principal inhibitor of apoptosis dependent on p53 [41]. Its downregulation by the extract could help overcome resistance mechanisms in breast cancer therapy by restoring cell cycle progression, sensitizing cancer cells to apoptotic signals, and potentially reducing tumor cell survival. Cells exposed to doxorubicin-induced apoptosis are known to be protected by p21 overexpression [42]. This gene serves as a negative regulator of *P53*, and knocking down the *CDKN1A* gene can increase *P53* regulation, such as induction by doxorubicin [43]. A significant increase in *CDKN1A* expression, up to 9.4 fold, has also been observed in MCF-7/D320 cells or doxorubicin-resistant MCF-7 cells [44].

We acknowledge several limitations in the present study. First, the findings in the present study were not validated by in vivo experiment. Although in vitro validation confirmed the modulatory effects of the extract, the system did not fully represent the complex physiological responses observed in vivo. Moreover, the analysis was limited to mRNA expression rather than protein levels, which may not fully reflect the actual functional or regulatory effects at the protein level. Additionally, the study assessed only the crude extract without further separation of pure phytocompounds, making it difficult to determine which specific compounds contributed to the observed effects.

Conclusion

The extract of *Ziziphus nummularia* stem demonstrates potential as an anticancer agent by inhibiting the proliferation of MCF-7 cells. Molecular docking and molecular dynamics simulations identify squalene and nummularine B as potential TP53RK inhibitors, further supported by decreased *CDKN1A* (*p21*) mRNA expression, a key downstream gene in the p53 signaling pathway. The inhibition of the p53 pathway does not prevent cellular senescence or cell cycle arrest, as evidenced by the downregulation of *CycE* (*CCNE1*), *RBL1*, and *E2F1*. These findings suggest a selective mechanism of action in which specific downstream genes are targeted without disrupting broader cellular processes of aging and cell cycle regulation. Further studies should explore the long-term impact of *Z. nummularia* stem metabolites on cellular senescence and cell cycle progression. Investigating the potential synergy of rutin, squalene, and nummularine B with other anticancer agents may also provide insights into their combined therapeutic potential. Additionally, in vivo studies are recommended to validate anticancer efficacy and safety profile of *Z. nummularia* stem metabolites.

Ethics approval

Not required.

Acknowledgments

Authors appreciate the technical and theoretical assistance from the Bioinformatics Core Facilities, Indonesia Medical Education and Research Institute, Faculty of Medicine, Universitas Indonesia.

Competing interests

The authors declare no conflict of interest.

Funding

We thank the Hibah Publikasi Terindeks Internasional (PUTI) Q2 Tahun Anggaran 2023—2024, Grant Number : NKB-683/UN2.RST/HKP.05.00/2023.

Underlying data

Derived data supporting the findings of this study are available from the corresponding author on request.

Declaration of artificial intelligence use

We hereby confirm that no artificial intelligence (AI) tools or methodologies were utilized at any stage of this study, including during data collection, analysis, visualization, or manuscript preparation. All work presented in this study was conducted manually by the authors without the assistance of AI-based tools or systems.

How to cite

Elya B, Rosmalena R, Fajrin AM, *et al*. Ethanol extract from *Ziziphus nummularia* stem inhibits MCF-7 breast cancer cell proliferation through TP53 regulating kinase (TP53RK)-mediated p53 activation: In silico and genes expression investigations. Narra J 2025; 5 (1): e1382 - http://doi.org/10.52225/narra.v5i1.1382.

References

1. Sung H, Ferlay J, Siegel RL, *et al*. Global cancer statistics 2020: GLOBOCAN estimates of incidence and mortality worldwide for 36 cancers in 185 countries. CA Cancer J Clin 2021;71(3):209-249.
2. Glajcar A, Łazarczyk A, Tyrak KE, *et al*. Nodal status in luminal A invasive breast cancer: Relationships with cytotoxic CD8 + and regulatory FOXP3 + cells tumor-associated infiltrate and other prognostic factors. Virchows Arch 2021;479(5):871-882.

3. Fernandes L, de Matos LV, Cardoso D, *et al*. Endocrine therapy for the treatment of leptomeningeal carcinomatosis in luminal breast cancer: A comprehensive review. CNS Oncol 2020;9(4):CNS65.
4. Davies C, Pan H, Godwin J, *et al*. Adjuvant tamoxifen: Longer against shorter (ATLAS) collaborative group. Long-term effects of continuing adjuvant tamoxifen to 10 years versus stopping at 5 years after diagnosis of oestrogen receptor-positive breast cancer: ATLAS, a randomised trial. Lancet 2013;381(9869):805-816.
5. Anderson DH. Luminal a breast cancer resistance mechanisms and emerging treatments. In: Freywald A, Franco J. Biological mechanisms and the advancing approaches to overcoming cancer drug resistance. London: Elsevier; 2021.
6. Szostakowska M, Trębińska-Stryjewska A, Grzybowska EA, Fabisiewicz A. Resistance to endocrine therapy in breast cancer: Molecular mechanisms and future goals. Breast Cancer Res Treat 2019;173(3):489-497.
7. Shanmugam MK, Sethi G. Molecular mechanisms of cell death. In: Liao D, editor. Mechanisms of cell death and opportunities for therapeutic development. Amsterdam: Academic Press; 2021.
8. Cerella C, Grandjenette C, Dicato M, Diederich M. Roles of apoptosis and cellular senescence in cancer and aging. Curr Drug Targets 2016;17(4):405-415.
9. Sazonova EV, Kopeina GS, Imyanitov EN, Zhivotovsky B. Platinum drugs and taxanes: Can we overcome resistance? Cell Death Discov 2021:7(1);155.
10. Voskarides K, Giannopoulou N. The role of TP53 in adaptation and evolution. Cells 2023;12(3):512.
11. Bazhanova E, Teply D. The apoptosis regulation mechanisms in hypothalamic neurons in physiological and pathological (Overexpression of Oncogene HER-2/Neu) aging. In: Baloyannis SJ, Gordeladze O, editors. Hypothalamus in health and diseases. Croatia: IntechOpen; 2018.
12. Rufini A, Tucci P, Celardo I, Melino G. Senescence and aging: The critical roles of p53. Oncogene 2013;32(43):5129-5143.
13. Capra M, Nuciforo PG, Confalonieri S, *et al*. Frequent alterations in the expression of serine/threonine kinases in human cancers. Cancer Res 2006;66(16):8147-8154.
14. Hideshima T, Chauhan D, Shima Y, *et al*. Thalidomide and its analogs overcome drug resistance of human multiple myeloma cells to conventional therapy. Blood 2000;96(9):2943-2950.
15. Sarvaiya HA, Yoon JH, Lazar IM. Proteome profile of the MCF7 cancer cell line: A mass spectrometric evaluation. Rapid Commun Mass Spectrom 2006;20(20):3039-3055.
16. Hideshima T, Cottini F, Nozawa Y, *et al*. p53-related protein kinase confers poor prognosis and represents a novel therapeutic target in multiple myeloma. Blood 2017;129(10):1308-1319.
17. Mombach JC, Bugs CA, Chaouiya C. Modelling the onset of senescence at the G1/S cell cycle checkpoint. BMC Genomics 2014;15(Suppl 7):S7.
18. Ara H, Hassan Md A, Khanam M. Taxonomic study of the genus *Ziziphus* Mill. (Rhamnaceae) of Bangladesh. Bangladesh J Plant Taxon 2008;15(1):47-61.
19. Mesmar J, Abdallah R, Badran A, *et al*. *Ziziphus nummularia*: A comprehensive review of its phytochemical constituents and pharmacological properties. Molecules 2022:27(13):4240.
20. Mesmar J, Fardoun MM, Abdallah R, *et al*. *Ziziphus nummularia* attenuates the malignant phenotype of human pancreatic cancer cells: Role of ROS. Molecules 2021;26(14):4295.
21. Padalia H, Chanda S. Antioxidant and anticancer activities of gold nanoparticles synthesized using aqueous leaf extract of *Ziziphus nummularia*. BioNanoScience 2021;11(2);281-294.
22. Abedini MR, Erfanian N, Nazem H, *et al*. Anti-proliferative and apoptotic effects of *Ziziphus* Jujube on cervical and breast cancer cells. Avicenna J Phytomed 2016;6(2):142-148.
23. Hashem DF, Hassani A, Nayeri N, *et al*. Anti-proliferative and apoptotic effects of aqueous extract of *Ziziphus* Jujube in human thyroid carcinoma cell lines (C643). Int J Cancer Manag 2018;11(7):e65820.
24. Ghaffari K, Ahmadi R, Saberi B, Moulavi P. Anti-proliferative effects of *Ziziphus* spina-christi and *Phlomis russeliana* leaf extracts on HEK293 and MCF-7 cell lines and evaluation of bax and Bcl-2 genes expression level in MCF-7 cells. Asian Pac J Cancer Prev 2021;22(S1):81-87.
25. Abedini MR, Erfanian N, Nazem H, *et al*. Anti-proliferative and apoptotic effects of *Ziziphus* Jujube on cervical and breast cancer cells. Avicenna J Phytomed 2016;6(2):142-148.
26. Abdallah R, Shaito AA, Badran A, *et al*. Fractionation and phytochemical composition of an ethanolic extract of *Ziziphus nummularia* leaves: Antioxidant and anticancerous properties in human triple negative breast cancer cells. Front Pharmacol 2024;15:1331843.
27. Martinez CA, Cistulli PA, Cook KM. A cell culture model that mimics physiological tissue oxygenation using oxygen-permeable membranes. Bio Protoc 2019;9(18):e3371.

28. Livak KJ, Schmittgen TD. Analysis of relative gene expression data using real-time quantitative PCR and the 2(-Delta Delta C(T)) Method. Methods 2001;25(4):402-408.
29. Pfaffl MW, Horgan GW, Dempfle L. Relative expression software tool (REST) for group-wise comparison and statistical analysis of relative expression results in real-time PCR. Nucleic Acids Res 2002;30(9):e36.
30. Kim S, Chen J, Cheng T, *et al*. PubChem 2023 update. Nucleic Acids Res 2023;51(D1):D1373-D1380.
31. Sander T, Freyss J, von Korff M, Rufener C. DataWarrior: An open-source program for chemistry aware data visualization and analysis. J Chem Inf Modeling 2015;55(2):460-473.
32. Li J, Ma X, Banerjee S, *et al*. Crystal structure of the human PRPK-TPRKB complex. Commun Biol 2021;4(1):167.
33. Bitencourt-Ferreira G, de Azevedo WF. Molegro virtual docker for docking. Methods Mol Biol 2019;2053:149-167.
34. Detering C, Varani G. Validation of automated docking programs for docking and database screening against RNA drug targets. J Med Chem 2004;47(17):4188-4201.
35. Molegro ApS. Molegro virtual docker user manual. Høegh-Guldbergs Gade 10, Building 1090 DK-8000 Aarhus C Denmark; 2011. Available from: http://molexus.io/molegro/MVD_Manual.pdf. Accessed: 17 April 2024.
36. Arsianti A, Nur Azizah N, Erlina L. Molecular docking, ADMET profiling of gallic acid and its derivatives (N-alkyl gallamide) as apoptosis agent of breast cancer MCF-7 Cells. F1000Res 2024;11:1453.
37. Castro-Alvarez A, Costa AM, Vilarrasa J. The performance of several docking programs at reproducing protein-macrolide-like crystal structures. Molecules 2017;22(1):136.
38. Fang Z, Lin M, Chen S, *et al*. E2F1 promotes cell cycle progression by stabilizing spindle fiber in colorectal cancer cells. Cell Mol Biol Lett 2022;27(1):90.
39. Song BN, Kim SK, Chu IS. Bioinformatic identification of prognostic signature defined by copy number alteration and expression of CCNE1 in non-muscle invasive bladder cancer. Exp Mol Med 2017;49(1):e282.
40. Zheng X, Chen L, Liu W, *et al*. CCNE1 is a predictive and immunotherapeutic indicator in various cancers including UCEC: a pan-cancer analysis. Hereditas 2023;160(1):13.
41. Gartel AL, Tyner AL. The role of the cyclin-dependent kinase inhibitor p21 in apoptosis. Mol Cancer Ther 2002;1(8):639-649.
42. AbuHammad S, Zihlif M. Gene expression alterations in doxorubicin resistant MCF7 breast cancer cell line. Genomics 2013;101(4):213-220.
43. Broude EV, Demidenko ZN, Vivo C, *et al*. p21 (CDKN1A) is a negative regulator of p53 stability. Cell Cycle 2007;6(12):1468-1471.
44. Bunz F, Hwang PM, Torrance C, *et al*. Disruption of p53 in human cancer cells alters the responses to therapeutic agents. J Clin Invest 1999;104(3):263-269.